Available online at www.sciencedirect.com
SCIENCE DIRECT®
Journal of Sound and Vibration 262 (2003) 1113–1131
JOURNAL OF SOUND AND VIBRATION
www.elsevier.com/locate/jsvi

Vibration analysis of planar serial-frame structures

H.P. Lin*, J. Ro

Department of Mechanical and Automation Engineering, Da-Yeh University, 112 Shan-Jiau Rd., Da-Tsuen, Chang-Hua 51505, Taiwan, ROC

Received 8 April 2002; accepted 1 July 2002

Abstract

A hybrid analytical/numerical method is proposed that permits the efficient dynamic analysis of planar serial-frame structures. The method utilizes a numerical implementation of a transfer matrix solution to the equation of motion. By analyzing the transverse and longitudinal motions of each segment simultaneously and considering the compatibility requirements across each frame angle, the undetermined variables of the entire frame structure system can be reduced to six which can be determined by application of the boundary conditions. The main feature of this method is to decrease the dimensions of the matrix involved in the finite element methods and certain other analytical methods.

1. Introduction

Frame structures are usually used in engineering designs, i.e., cranes, bridges, aerospace structures, etc. The dynamic behaviors of frame structures can be predicted by using certain analytical and numerical methods such as the dynamic stiffness methods (DSM) and the finite element methods (FEM). The DSM employs the solutions of governing equations under harmonic nodal excitations as shape functions to formulate an analytical stiffness matrix. The method requires closed-form solutions of the governing equations which restrict the application areas [1]. The FEM has been very commonly used in recent years in this field. However, the FEM requires a large amount of computer memory and computation time, since many degrees of freedom are required for accurately solving dynamic problems for these structures [2,3]. To solve this problem, various methods have been studied to overcome the disadvantages [2–5]. In most of the previous studies, the Euler–Bernoulli beam-theory model obtained by deriving the differential equation and the associated boundary conditions for a basic uniform Euler–Bernoulli beam are

*Corresponding author. Tel.: +886-4-8511888; fax: +886-4-8511895.
E-mail address: linhp@mail.dyu.edu.tw (H.P. Lin).

0022-460X/03/$ - see front matter
PII: S0022-460X(02)01089-1

often used and discussed. Some researchers have also studied the different results between the Euler–Bernoulli beam-theory models and the Timoshenko beam theory. Finally, it is possible to evaluate natural frequencies simply by finding roots of the *high order determinant* of the coefficient matrix of the linear system if accuracy of the eigensolutions is required.

This investigation presents a hybrid analytical/numerical method that permits the efficient computation of the eigensolutions for planar serial-frame structures with various boundary conditions. The method is based on partitioning the frame structure to the sub-beam segments and considering the transverse and longitudinal motions of each segment and, by the compatibility requirements across each frame angle, the relationship of the six integration constants of the eigenfunctions between adjacent sub-beams can be determined. By using the transfer matrix method [9,10], as a consequence, the entire system has only six unknown constants, which can be solved through the satisfaction of six boundary conditions. In this article, the eigenvalue problem is solved by using closed-form transfer matrix methods.

2. Theoretical model

A typical planar serial-frame structure with K frame angles $\theta_1, \theta_2, \ldots, \theta_K$ is shown in Fig. 1. This structure is partitioned into $K+1$ components at the angle positions enabling a substructure approach. There are $K+1$ sub-beams with lengths $L_1, L_2, \ldots, L_{K+1}$, and the positions of the frame angles are located by $X_1, X_2, ..., X_K$, respectively, in Fig. 1. In doing the vibration analysis of this system for this study, each component member (sub-beam) is analyzed by its transverse and longitudinal motions, respectively. Let the X-axis represent the longitudinal direction and the Y-axis the transverse direction of each component member; then, the traditional vibration theories of an Euler–Bernoulli beam and the axial vibration of a rod are considered. The vibration amplitudes of the transverse and longitudinal displacements of the component i (sub-beam) are

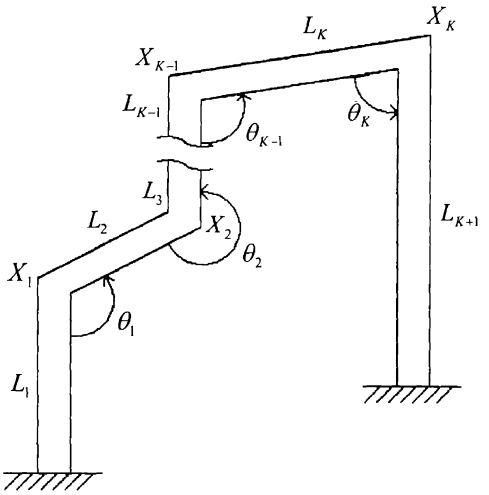

Fig. 1. A planar serial-frame structure with K frame angles $\theta_1, \theta_2, \ldots, \theta_k$ located at positions $X_1, X_2, \ldots, X_K$, respectively; lengths of sub-beams are $L_1, L_2, \ldots, L_k, L_{k+1}$ where $L_1 + L_2 + \cdots + L_k + L_{k+1} = L$.

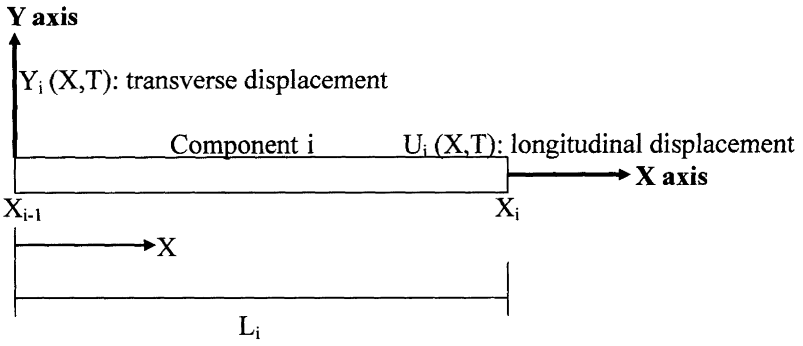

Fig. 2. Transverse and longitudinal motions of a segment.

denoted by $Y_i(X,T)$ and $U_i(X,T)$ on the interval $X_{i-1} < X < X_i$ where the sub-index i represents the ith segment and $i = 1, 2, \ldots, K+1$, as shown in Fig. 2. The entire system is now divided into $K+1$ segments, wherein the total length of this frame system is $L\,(= L_1 + L_2 + \cdots + L_{K+1})$. According to Refs. [6–8], the equations of motion for each segment, assumed with a uniform cross-section, are

transverse motion:

$$EI\frac{\partial^4 Y_i(X,T)}{\partial X^4} + \rho A\frac{\partial^2 Y_i(X,T)}{\partial T^2} = 0, \quad X_{i-1} < X < X_i, \quad i = 1, 2, \ldots, K+1, \tag{1}$$

longitudinal motion:

$$E\frac{\partial^2 U_i(X,T)}{\partial X^2} - \rho\frac{\partial^2 U_i(X,T)}{\partial T^2} = 0, \quad X_{i-1} < X < X_i, \quad i = 1, 2, \ldots, K+1, \tag{2}$$

where E is Young's modulus of the material, I is the moment of inertia of the beam cross-section, ρ is the density of material and A is the cross-section area of the beam.

The boundary conditions, the fixed–fixed supported case for this example, are

$$Y(0,T) = Y(L,T) = 0, \tag{3a}$$

$$Y'(0,T) = Y'(L,T) = 0, \tag{3b}$$

$$U(0,T) = U(L,T) = 0. \tag{3c}$$

The transverse and the longitudinal motions at the end of the segment before each frame angle constrain the motions of the adjacent segment after the same frame angle. So the "compatibility conditions" enforce continuities in the displacement field (in both transverse and longitudinal), slope, bending moment, shear force and axial force, respectively, across each frame angle θ_i, as shown in Fig. 3a (displacements) and Fig. 3b (forces), which can be expressed as

$$Y_{i+1}(X_i^+,T) = -Y_i(X_i^-,T)\cos\theta_i + U_i(X_i^-,T)\sin\theta_i, \quad \text{displacement continuity}, \tag{4a}$$

$$U_{i+1}(X_i^+,T) = -Y_i(X_i^-,T)\sin\theta_i + U_i(X_i^-,T)\cos\theta_i, \quad \text{displacement continuity}, \tag{4b}$$

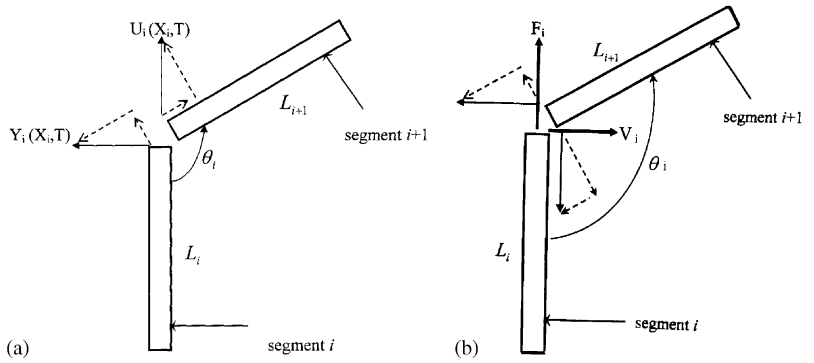

Fig. 3. (a) Displacement compatibility requirements across ith frame angle θ_i: Y_i and U_i are transverse and longitudinal displacements of segment i at position X_i. (b) Force compatibility requirements across ith frame angle θ_i: V_i and F_i are shear and axial forces of segment i at position X_i.

$$Y'_{i+1}(X_i^+, T) = Y'_i(X_i^-, T), \quad \text{slope continuity,} \tag{4c}$$

$$Y''_{i+1}(X_i^+, T) = Y''_i(X_i^-, T), \quad \text{moment continuity,} \tag{4d}$$

$$EIY'''_{i+1}(X_i^+, T) = -EIY'''_i(X_i^-, T)\cos\theta_i - EAU'_i(X_i^-, T)\sin\theta_i, \quad \text{shear continuity,} \tag{4e}$$

$$EAU'_{i+1}(X_i^+, T) = EIY'''_i(X_i^-, T)\sin\theta_i - EAU'_i(X_i^-, T)\cos\theta_i, \quad \text{axial force continuity,} \tag{4f}$$

where the symbols X_i^+ and X_i^- denote the locations immediately above and below the angle position X_i. All the assumptions in the above compatibility conditions are the same as the traditional analysis of the transverse vibrations of an Euler–Bernoulli beam and the axial vibrations of a rod. The frame angles are also assumed to be unchanged during the motions of the frame.

In the above, the following quantities are introduced:

$$y = \frac{Y}{L}, \quad x = \frac{X}{L}, \quad u = \frac{U}{L}, \quad t = \frac{T}{\sqrt{L}}, \quad l_i = \frac{L_i}{L}, \quad x_i = \frac{X_i}{L}. \tag{5}$$

Thus, in each segment, Eqs. (1) and (2) can then be expressed in a non-dimensional form as

$$\frac{EI}{L^3}\frac{\partial^4 y_i(x,t)}{\partial x^4} + \rho A\frac{\partial^2 y_i(x,t)}{\partial t^2} = 0, \quad x_{i-1} < x < x_i, \quad i = 1, 2, \ldots, K+1, \tag{6}$$

$$\frac{E}{L}\frac{\partial^2 u_i(x,t)}{\partial x^2} - \rho\frac{\partial^2 u_i(x,t)}{\partial t^2} = 0, \quad x_{i-1} < x < x_i, \quad i = 1, 2, \ldots, K+1. \tag{7}$$

The non-dimensional "compatibility conditions" across each frame angle are (from Eqs. (4a)–(4f))

$$y_{i+1}(x_i^+, t) = -y_i(x_i^-, t)\cos\theta_i + u_i(x_i^-, t)\sin\theta_i, \tag{8a}$$

$$u_{i+1}(x_i^+, t) = -y_i(x_i^-, t)\sin\theta_i - u_i(x_i^-, t)\cos\theta_i, \tag{8b}$$

$$y'_{i+1}(x_i^+, t) = y'_i(x_i^-, t), \tag{8c}$$

$$y''_{i+1}(x_i^+, t) = y''_i(x_i^-, t), \tag{8d}$$

$$y'''_{i+1}(x_i^+, t) = -y'''_i(x_i^-, t)\cos\theta_i - \frac{AL^2}{I}u'_i(x_i^-, t)\sin\theta_i, \tag{8e}$$

$$u'_{i+1}(x_i^+, t) = \frac{I}{AL^2}y'''_i(x_i^-, t)\sin\theta_i - u'_i(x_i^-, t)\cos\theta_i, \tag{8f}$$

where $i = 1, 2, ..., K$. Similarly, the non-dimensional boundary conditions from Eqs. (3a)–(3c), for the example of fixed–fixed ends, can be written as

$$y(0, t) = y(1, t) = 0, \tag{9a}$$

$$y'(0, t) = y'(1, t) = 0, \tag{9b}$$

$$u(0, t) = u(1, t) = 0. \tag{9c}$$

3. Calculation of eigensolutions

The eigensolutions for cases of commonly used different boundary conditions are derived. The solutions of the other boundary conditions can also be obtained easily through a similar procedure. Using the separable solutions: $y_i(x, t) = w_i(x)e^{j\omega t}$ and $u_i(x, t) = v_i(x)e^{j\omega t}$ in Eqs. (6) and (7) leads to an associated eigenvalue problem,

$$w_i''''(x) - \lambda^4 w_i(x) = 0, \quad x_{i-1} < x < x_i, \quad i = 1, 2, \ldots, K+1, \tag{10}$$

$$v_i''(x) + \gamma^2 v_i(x) = 0, \quad x_{i-1} < x < x_i, \quad i = 1, 2, \ldots, K+1, \tag{11}$$

where

$$\lambda^4 = \frac{\rho AL^3\omega^2}{EI} \quad \text{and} \quad \gamma^2 = \frac{\rho L\omega^2}{E}. \tag{12}$$

From Eq. (12), the relationship between λ and γ can be expressed as

$$\gamma = \sqrt{\frac{I}{A}}\frac{1}{L}\lambda^2 = a\lambda^2, \tag{13}$$

where a is a constant ($a = \sqrt{I/A}\,(1/L)$); for a square cross-section of the segment with width B and height H, a can be expressed as $a = \sqrt{I/A}(1/L) = \sqrt{1/12}(H/L)$. From Eqs. (8a)–(8f), the corresponding compatibility conditions across each frame angle lead to

$$w_{i+1}(x_i^+) = -w_i(x_i^-)\cos\theta_i + v_i(x_i^-)\sin\theta_i, \tag{14a}$$

$$v_{i+1}(x_i^+) = -w_i(x_i^-)\sin\theta_i - v_i(x_i^-)\cos\theta_i, \tag{14b}$$

$$w'_{i+1}(x_i^+) = w'_i(x_i^-), \tag{14c}$$

$$w''_{i+1}(x_i^+) = w''_i(x_i^-), \tag{14d}$$

$$w'''_{i+1}(x_i^+) = -w'''_i(x_i^-)\cos\theta_i - \frac{AL^2}{I}v'_i(x_i^-)\sin\theta_i, \tag{14e}$$

$$v'_{i+1}(x_i^+) = \frac{I}{AL^2}w'''_i(x_i^-)\sin\theta_i - v'_i(x_i^-)\cos\theta_i \tag{14f}$$

for $i = 1, 2, \ldots, K$. The boundary conditions, from Eqs. (9a)–(9c), are

$$w(0) = 0, \quad w(1) = 0, \quad w'(0) = 0, \tag{15a–c}$$

$$w'(1) = 0, \quad v(0) = 0, \quad v(1) = 0. \tag{15d–f}$$

A closed-form solution to this eigenvalue problem can be obtained by employing transfer matrix methods [9,10]. The general solutions of Eqs. (10) and (11), for each segment, are

$$\begin{aligned} w_i(x) = {} & A_i\sin\lambda(x - x_{i-1}) + B_i\cos\lambda(x - x_{i-1}) + C_i\sinh\lambda(x - x_{i-1}) \\ & + D_i\cosh\lambda(x - x_{i-1}), \quad x_{i-1} < x < x_i, \quad i = 1, 2, \ldots, K+1, \end{aligned} \tag{16}$$

$$\begin{aligned} v_i(x) &= E_i\sin\gamma(x - x_{i-1}) + F_i\cos\gamma(x - x_{i-1}) \\ &= E_i\sin a\lambda^2(x - x_{i-1}) + F_i\cos a\lambda^2(x - x_{i-1}), \quad x_{i-1} < x < x_i, \quad i = 1, 2, \ldots, K+1, \end{aligned} \tag{17}$$

where A_i, B_i, C_i, D_i, E_i and F_i are constants associated with the ith segment ($i = 1, 2, \ldots, K+1$). The constants in the $(i+1)$th segment (A_{i+1}, B_{i+1}, C_{i+1}, D_{i+1}, E_{i+1} and F_{i+1}) are related to those in the ith segment (A_i, B_i, C_i, D_i, E_i and F_i) through the compatibility conditions in Eqs. (14a)–(14f), which can be expressed as

$$\begin{Bmatrix} A_{i+1} \\ B_{i+1} \\ C_{i+1} \\ D_{i+1} \\ E_{i+1} \\ F_{i+1} \end{Bmatrix} = \begin{bmatrix} t_{11} & t_{12} & t_{13} & t_{14} & t_{15} & t_{16} \\ \vdots & & & & & \\ \vdots & & & & & \\ \ldots & & & & t_{65} & t_{66} \end{bmatrix}^{(i)} \begin{Bmatrix} A_i \\ B_i \\ C_i \\ D_i \\ E_i \\ F_i \end{Bmatrix} = \underline{T}^{(i)}_{6\times 6} \begin{Bmatrix} A_i \\ B_i \\ C_i \\ D_i \\ E_i \\ F_i \end{Bmatrix}, \tag{18}$$

where $\underline{T}^{(i)}_{6\times 6}$ is the 6×6 transfer matrix which depends on the eigenvalue λ, for which the elements are derived in Appendix A.

Through repeated applications of Eq. (18), the six constants in the first segment (A_1, B_1, C_1, D_1, E_1 and F_1) can be mapped into those of the last segment, thereby reducing the number of independent constants of the entire system to six:

$$\begin{Bmatrix} A_{K+1} \\ B_{K+1} \\ C_{K+1} \\ D_{K+1} \\ E_{K+1} \\ F_{K+1} \end{Bmatrix} = \underline{T}^{(K)}_{6\times6} \begin{Bmatrix} A_K \\ B_K \\ C_K \\ D_K \\ E_K \\ F_K \end{Bmatrix} = \underline{T}^{(K)}_{6\times6}\, \underline{T}^{(K-1)}_{6\times6} \begin{Bmatrix} A_{K-1} \\ B_{K-1} \\ C_{K-1} \\ D_{K-1} \\ E_{K-1} \\ F_{K-1} \end{Bmatrix} = \underline{T}^{(K)}_{6\times6}\, \underline{T}^{(K-1)}_{6\times6} \cdots \underline{T}^{(1)}_{6\times6} \begin{Bmatrix} A_1 \\ B_1 \\ C_1 \\ D_1 \\ E_1 \\ F_1 \end{Bmatrix}. \tag{19}$$

These six remaining constants (A_1, B_1, C_1, D_1, E_1 and F_1) can be determined through the satisfaction of the boundary conditions in Eqs. (15a)-(15f). For the example case of a planar serial-frame with fixed–fixed ends, beginning with those at the left support, Eqs. (16), (17), (15a), (15c) and (15e) lead to

$$B_1 + D_1 = 0, \quad A_1 + C_1 = 0, \quad F_1 = 0. \tag{20a–c}$$

Satisfaction of the boundary conditions of Eqs. (16) and (17) at the right support, Eqs. (15b), (15d) and (15f), requires

$$A_{K+1} \sin \lambda l_{K+1} + B_{K+1} \cos \lambda l_{K+1} + C_{K+1} \sinh \lambda l_{K+1} + D_{K+1} \cos h\lambda l_{K+1} = 0, \tag{20d}$$

$$A_{K+1} \cos \lambda l_{K+1} - B_{K+1} \sin \lambda l_{K+1} + C_{K+1} \cosh \lambda l_{K+1} + D_{K+1} \sinh \lambda l_{K+1} = 0, \tag{20e}$$

$$E_{K+1} \sin a\lambda^2 l_{K+1} + F_{K+1} \cos a\lambda^2 l_{K+1} = 0, \tag{20f}$$

which can be expressed in matrix form as

$$\begin{Bmatrix} 0 \\ 0 \\ 0 \end{Bmatrix} = \begin{bmatrix} \sin \lambda l_{K+1} & \cos \lambda l_{K+1} & \sinh \lambda l_{K+1} & \cosh \lambda l_{K+1} & 0 & 0 \\ \cos \lambda l_{K+1} & -\sin \lambda l_{K+1} & \cosh \lambda l_{K+1} & \sinh \lambda l_{K+1} & 0 & 0 \\ 0 & 0 & 0 & 0 & \sin a\lambda^2 l_{K+1} & \cos a\lambda^2 l_{K+1} \end{bmatrix} \times \begin{Bmatrix} A_{K+1} \\ B_{K+1} \\ C_{K+1} \\ D_{K+1} \\ E_{K+1} \\ F_{K+1} \end{Bmatrix} = \underline{B}_{3\times6} \begin{Bmatrix} A_{K+1} \\ B_{K+1} \\ C_{K+1} \\ D_{K+1} \\ E_{K+1} \\ F_{K+1} \end{Bmatrix}, \tag{21}$$

where

$$\underline{B}_{3\times6} = \begin{bmatrix} \sin \lambda l_{K+1} & \cos \lambda l_{K+1} & \sinh \lambda l_{K+1} & \cosh \lambda l_{K+1} & 0 & 0 \\ \cos \lambda l_{K+1} & -\sin \lambda l_{K+1} & \cosh \lambda l_{K+1} & \sinh \lambda l_{K+1} & 0 & 0 \\ 0 & 0 & 0 & 0 & \sin a\lambda^2 l_{K+1} & \cos a\lambda^2 l_{K+1} \end{bmatrix}. \tag{22}$$

Substitution of Eq. (19) into Eq. (21) and use of Eq. (20a)-(20c) leads to

$$\begin{Bmatrix} 0 \\ 0 \\ 0 \end{Bmatrix} = \underline{B}_{3\times 6} \begin{Bmatrix} A_{K+1} \\ B_{K+1} \\ C_{K+1} \\ D_{K+1} \\ E_{K+1} \\ F_{K+1} \end{Bmatrix} = \underline{B}_{3\times 6} \underline{T}^{(K)}_{6\times 6}\, \underline{T}^{(K-1)}_{6\times 6} \cdots \underline{T}^{(1)}_{6\times 6} \begin{Bmatrix} A_1 \\ B_1 \\ C_1 \\ D_1 \\ E_1 \\ F_1 \end{Bmatrix},$$

$$\begin{Bmatrix} 0 \\ 0 \\ 0 \end{Bmatrix} = \underline{R}_{3\times 6} \begin{Bmatrix} A_1 \\ B_1 \\ C_1 \\ D_1 \\ E_1 \\ F_1 \end{Bmatrix} = \begin{bmatrix} r_{11} & r_{12} & r_{13} & r_{14} & r_{15} & r_{16} \\ r_{21} & r_{22} & r_{23} & r_{24} & r_{25} & r_{26} \\ r_{31} & r_{32} & r_{33} & r_{34} & r_{35} & r_{36} \end{bmatrix} \begin{Bmatrix} A_1 \\ B_1 \\ -A_1 \\ -B_1 \\ E_1 \\ 0 \end{Bmatrix}, \tag{23}$$

where

$$\underline{R}_{3\times 6} = \underline{B}_{3\times 6}\, \underline{T}^{(K)}_{6\times 6}\, \underline{T}^{(K-1)}_{6\times 6} \cdots \underline{T}^{(1)}_{6\times 6} = \begin{bmatrix} r_{11} & r_{12} & r_{13} & r_{14} & r_{15} & r_{16} \\ r_{21} & r_{22} & r_{23} & r_{24} & r_{25} & r_{26} \\ r_{31} & r_{32} & r_{33} & r_{34} & r_{35} & r_{36} \end{bmatrix}.$$

Thus, the existence of non-trivial solutions requires

$$\det \begin{bmatrix} r_{11}(\lambda) - r_{13}(\lambda) & r_{12}(\lambda) - r_{14}(\lambda) & r_{15}(\lambda) \\ r_{21}(\lambda) - r_{23}(\lambda) & r_{22}(\lambda) - r_{24}(\lambda) & r_{25}(\lambda) \\ r_{31}(\lambda) - r_{33}(\lambda) & r_{32}(\lambda) - r_{34}(\lambda) & r_{35}(\lambda) \end{bmatrix} = 0. \tag{24}$$

This determinant provides the single (characteristic) equation for the solution of the eigenvalue λ_n. This equation is solved using the standard Newton–Raphson iterations or, for simplification, using the method shown in Fig. 4 to obtain the eigenvalues. The coefficients of the eigenfunctions, $w_n(x)$ and $v_n(x)$, are obtained by back-substitution into Eqs. (23) and (18) followed by Eqs. (16) and (17).

For cases of other usually used boundary conditions, through a similar procedure, the following relationships can be obtained:

(a) *Fixed–hinged boundary conditions*: The existence of non-trivial solutions for the constants A_1, B_1,C_1, D_1, E_1 and F_1 is the same as in Eq. (24), but the matrix $\underline{B}_{3\times 6}$ in Eq. (21) now becomes

$$\underline{B}_{3\times 6} = \begin{bmatrix} \sin \lambda l_{K+1} & \cos \lambda l_{K+1} & \sinh \lambda l_{K+1} & \cosh \lambda l_{K+1} & 0 & 0 \\ -\sin \lambda l_{K+1} & -\cos \lambda l_{K+1} & \sinh \lambda l_{K+1} & \cosh \lambda l_{K+1} & 0 & 0 \\ 0 & 0 & 0 & 0 & \sin a\lambda^2 l_{K+1} & \cos a\lambda^2 l_{K+1} \end{bmatrix}. \tag{25}$$

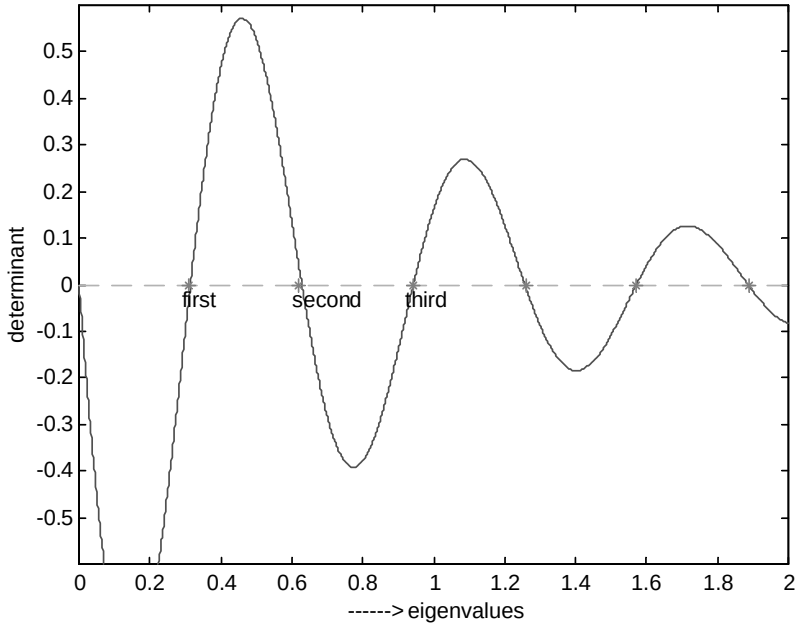

Fig. 4. Simple calculation of eigenvalues.

(b) *Fixed–free boundary conditions*: The existence of non-trivial solutions is the same as in Eq. (24), but the matrix $\underline{B}_{3\times6}$ in Eq. (21) now becomes

$$\underline{B}_{3\times6} = \begin{bmatrix} -\sin\lambda l_{K+1} & -\cos\lambda l_{K+1} & \sinh\lambda l_{K+1} & \cosh\lambda l_{K+1} & 0 & 0 \\ -\cos\lambda l_{K+1} & \sin\lambda l_{K+1} & \cosh\lambda l_{K+1} & \sinh\lambda l_{K+1} & 0 & 0 \\ 0 & 0 & 0 & 0 & \cos a\lambda^2 l_{K+1} & -\sin a\lambda^2 l_{K+1} \end{bmatrix}. \tag{26}$$

(c) *Hinged-hinged boundary conditions*: The existence of non-trivial solutions now requires

$$\det\begin{bmatrix} r_{11}(\lambda) & r_{13}(\lambda) & r_{15}(\lambda) \\ r_{21}(\lambda) & r_{23}(\lambda) & r_{25}(\lambda) \\ r_{31}(\lambda) & r_{33}(\lambda) & r_{35}(\lambda) \end{bmatrix} = 0, \tag{27}$$

the matrix $\underline{B}_{3\times6}$ in Eq. (21) is now the same as in Eq. (25).

(d) *Free–free boundary conditions*: The existence of non-trivial solutions requires

$$\det\begin{bmatrix} r_{11}(\lambda)+r_{13}(\lambda) & r_{12}(\lambda)+r_{14}(\lambda) & r_{16}(\lambda) \\ r_{21}(\lambda)+r_{23}(\lambda) & r_{22}(\lambda)+r_{24}(\lambda) & r_{26}(\lambda) \\ r_{31}(\lambda)+r_{33}(\lambda) & r_{32}(\lambda)+r_{34}(\lambda) & r_{36}(\lambda) \end{bmatrix} = 0, \tag{28}$$

and the matrix $\underline{B}_{3\times6}$ in Eq. (21) is now the same as Eq. (26).

4. Numerical results and discussion

In order to validate the method presented in this article, some numerical results are compared with the available and experimental data. First is the case of an angled-beam structure, as shown in Fig. 5. The case of $\theta_1 = \pi$ represents a straight beam, for which the numerical calculation results for different boundary conditions by the proposed solution procedure in this study are shown in Table 1. Table 1 shows that the above results are almost the same as the exact solutions for a beam in different boundary conditions. For another case of a fixed–free angled beam with $\theta_1 = \pi/2$, $L_1 = L_2 = 50\,\text{cm}$, section width $B = 12.7\,\text{mm}$, section height $H = 12.7\,\text{mm}$, density $\rho = 7800\,\text{kg/m}^3$, Young's modulus $E = 2.06 \times 10^{11}\,\text{N/m}^2$, as shown in Fig. 6, by experimental modal testing, the lowest five natural frequencies of this structure are measured as $\Omega_1 = 14\,\text{Hz}$, $\Omega_2 = 38\,\text{Hz}$, $\Omega_3 = 184\,\text{Hz}$, $\Omega_4 = 269\,\text{Hz}$ and $\Omega_5 = 583\,\text{Hz}$. The comparisons of the calculated natural frequencies from this study and the measured results are shown in Table 2, which indicates that the errors are small and satisfactory.

For the case of $\theta_1 = \pi/2$ with a fixed–fixed boundary condition (Fig. 5), by changing the angle position l_1 (non-dimensional) from 0 to 1.0, the lowest four eigenvalues (natural frequencies) obtained in this study are shown in Fig. 7. In this case, Fig. 7 is symmetric because the results from angle position l_1 should be the same as the results from angle position $1 - l_1$. Also note that the solutions for the cases $l_1 = 0$ and 1.0 are the same as the cases of a straight beam with a fixed–fixed boundary condition. For the same structure with $l_1 = l_2 = 0.5$ (Fig. 5), by changing the frame angle θ_1 from 0° to 180°, the lowest four eigenvalues are obtained as shown in Fig. 8, which indicates that the variations in these lowest four eigenvalues are small when the angle θ_1 is in the

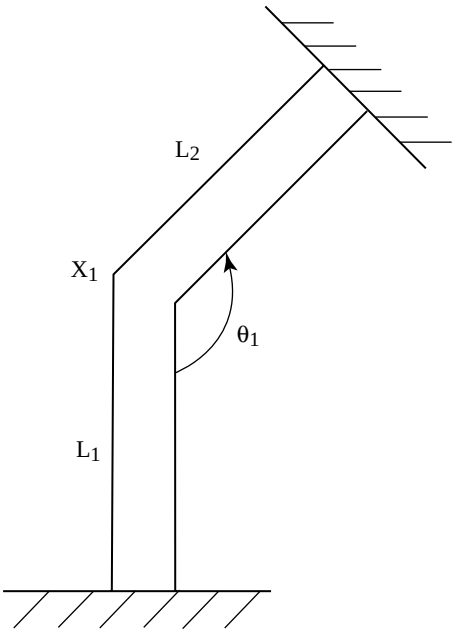

Fig. 5. An angled-beam structure with one frame angle.

Table 1
Comparisons for an angled-beam structure with angle $\theta_1 = 180^\circ$ ($H/L = 0.05$)

Different B.C's	Eigenvalues					
	λ_1		λ_2		λ_3	
	Calculated from this study	Exact solution	Calculated from this study	Exact solution	Calculated from this study	Exact solution
Hinged–hinged	3.1426	π	6.2842	2π	9.4258	3π
Fixed–free	1.8801	1.8735	4.6991	4.6736	7.8598	7.8549
Fixed–fixed	4.7350	4.7296	7.8582	7.8524	11.0006	10.9955

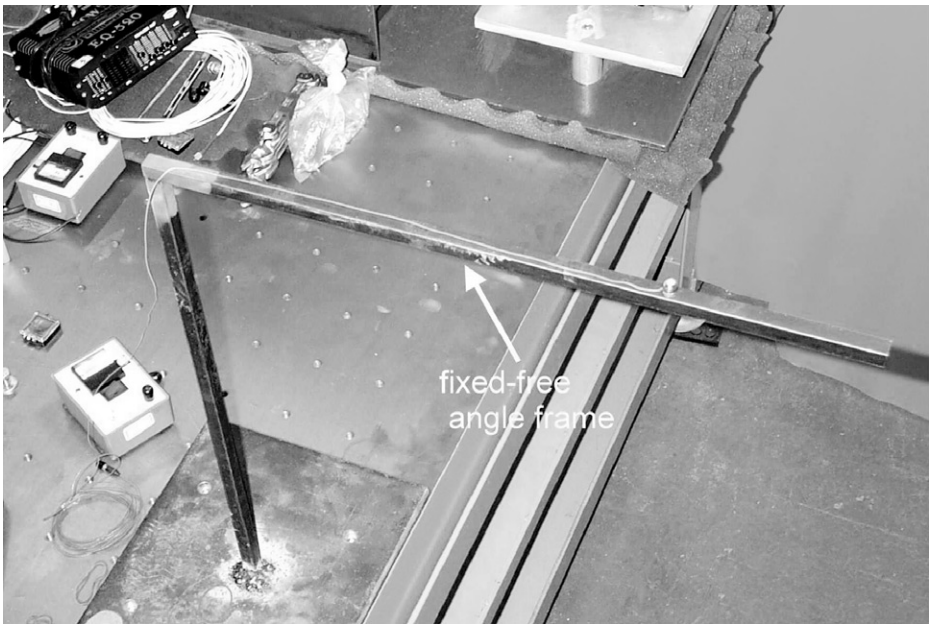

Fig. 6. An experimental fixed–free angled-beam structure.

range from 40° to 140°. It can be considered that the dynamic stiffness of this frame structure is close within this frame angle range. Also note that in Fig. 8, there is a "cross-over" phenomenon for the first and the second modes near the angle θ_1 above 160°. Before this cross-over point, the first mode is anti-symmetric and the second mode is symmetric in the transverse motion (dominant). After this cross-over point, the first mode now becomes symmetric and the second mode becomes anti-symmetric. This can be distinguished from the mode shapes shown in Figs. 9 and 10 for different θ_1 angles ($\theta_1 = 140^\circ, 160^\circ, 170^\circ$ and 180°). The third mode in Fig. 8 also has a

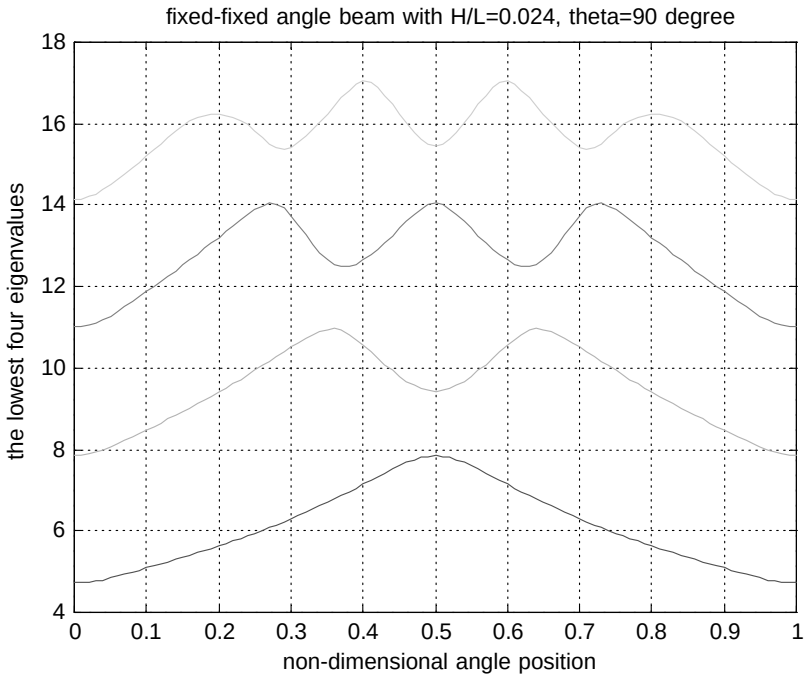

Fig. 7. Lowest four eigenvalues for an angled-beam structure by changing angle position l_1.

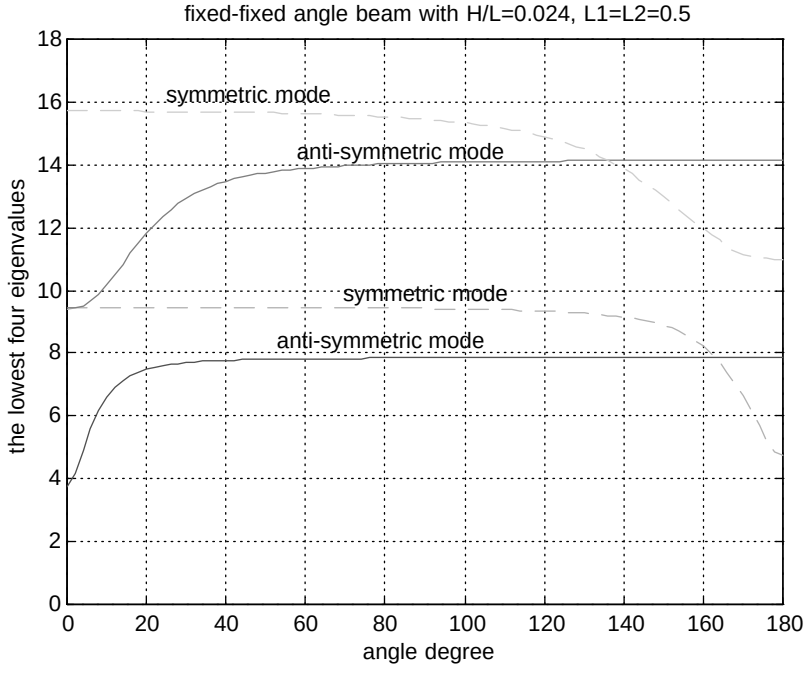

Fig. 8. Lowest four eigenvalues for an angled-beam structure by changing angle θ_1.

Table 2
Experimental comparisons of a fixed–free angled-beam structure with angle $\theta = \pi/2$, $L_1 = L_2 = 50\,\text{cm}$, section height $H = 1.27\,\text{cm}$, section width $B = 1.27\,\text{cm}$, density $\rho = 7800\,\text{kg/m}^3$ and Young's modulus, $E = 2.06 \times 10^{11}\,\text{N/m}^2$

Measured natural frequencies (Hz)	Calculated natural frequency	
	Calculated from this study (Hz)	Error (%)
$\Omega_1 = 14$	14.2	1.4
$\Omega_2 = 38$	38.3	0.79
$\Omega_3 = 184$	188.9	3.2
$\Omega_4 = 269$	276.6	2.8
$\Omega_5 = 583$	603.2	3.5

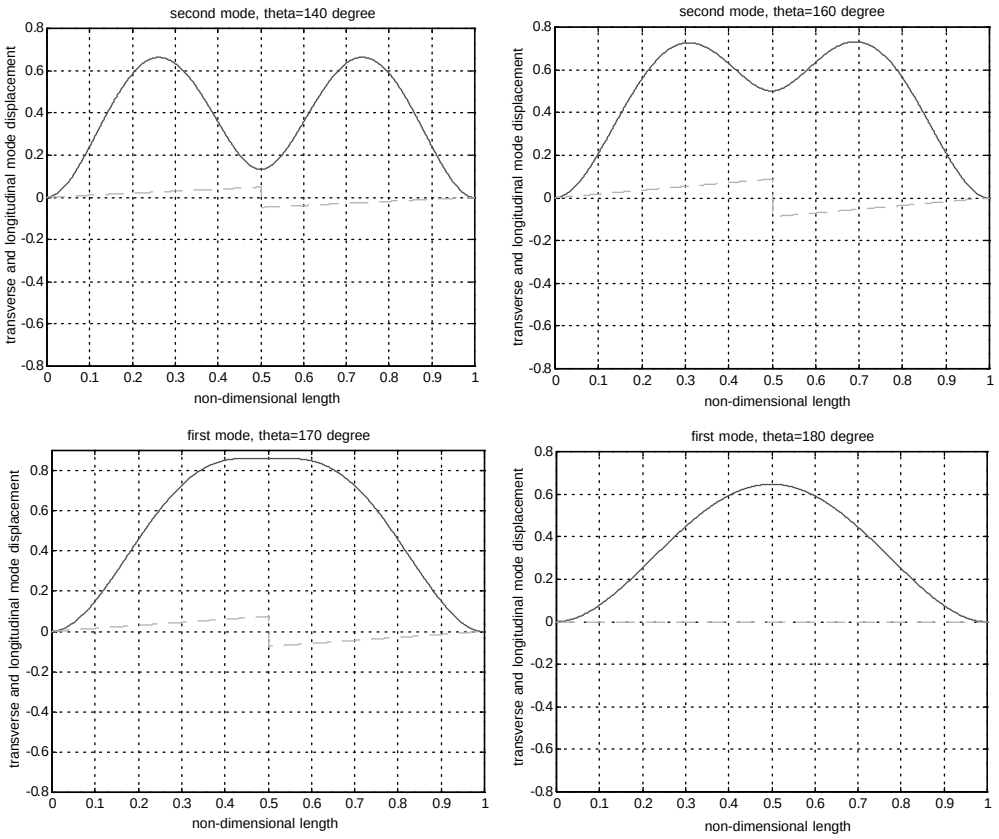

Fig. 9. Transverse symmetric mode shapes near cross-over point for $\theta_1 = 140^\circ$, 160°, 170°, and 180°: solid curve, transverse displacement; dashed curve, longitudinal displacement.

phenomenon similar to the first mode. There is also a "cross-over" point at the third and the fourth modes near the position θ_1 below 140°. The third mode shapes for different θ_1 values ($\theta_1 = 20^\circ, 30^\circ, 100^\circ, 140^\circ, 160^\circ$ and 180°) are shown in Fig. 11, which indicated that before the

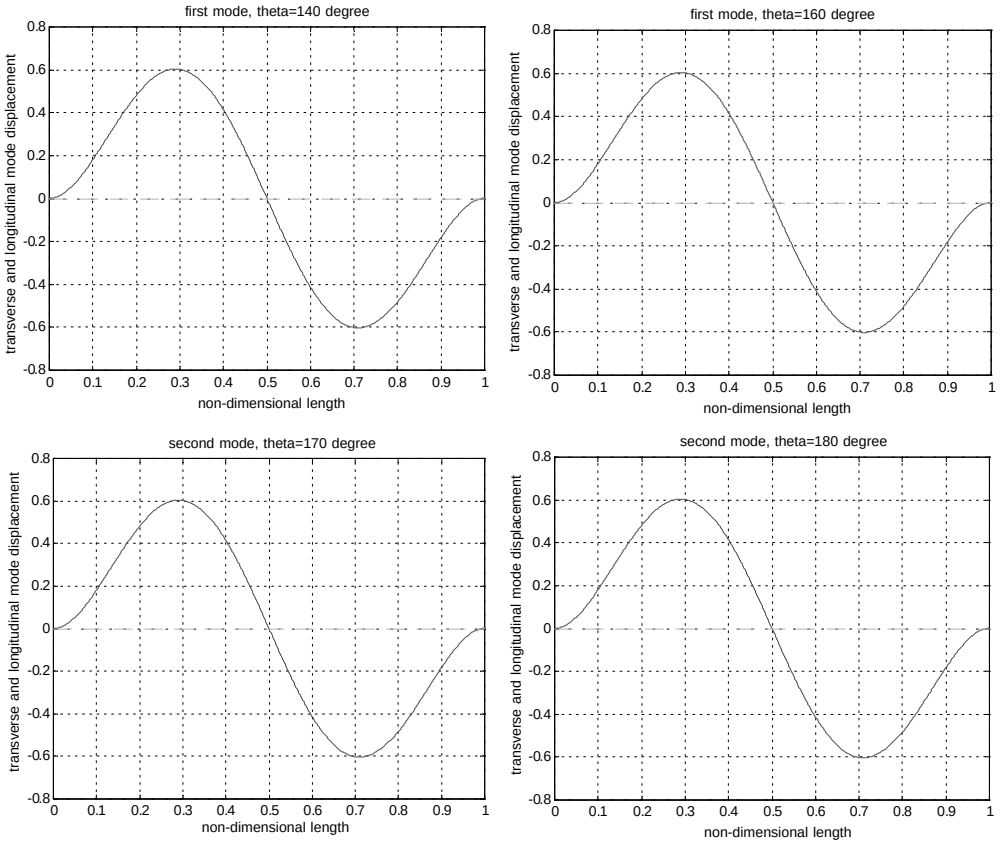

Fig. 10. Transverse anti-symmetric mode shapes near cross-over point for $\theta_1 = 140^\circ$, 160°, 170°, and 180°: solid curve, transverse displacement; dashed curve, longitudinal displacement.

cross-over point ($\theta_1 < 140^\circ$) the transverse motion of the third mode is anti-symmetric, and after this cross-over point the third mode becomes symmetric.

For a frame structure with multiple frame angles, as shown in Fig. 12a, by the proposed solution procedure in this study, the eigensolutions (natural frequencies and mode shapes) can easily be obtained. The geometry of the frame structure in Fig. 12a is $l_1 = 0.3$, $l_2 = 0.4$, $l_3 = 0.3$, $\theta_1 = \pi/2$, $\theta_2 = \pi/2$ with a fixed–fixed boundary condition. The lowest three eigenvalues are obtained as: $\lambda_1 = 5.5992$, $\lambda_2 = 9.5904$, $\lambda_3 = 14.3330$, the corresponding eigenfunctions (mode shapes) of which are shown in Figs. 12b–d.

5. Conclusions

A hybrid analytical/numerical solution method that permits the efficient evaluation of eigensolutions for planar serial-frame structures has been developed. The method utilizes a numerical implementation of a transfer matrix solution to the analytical equation of motion.

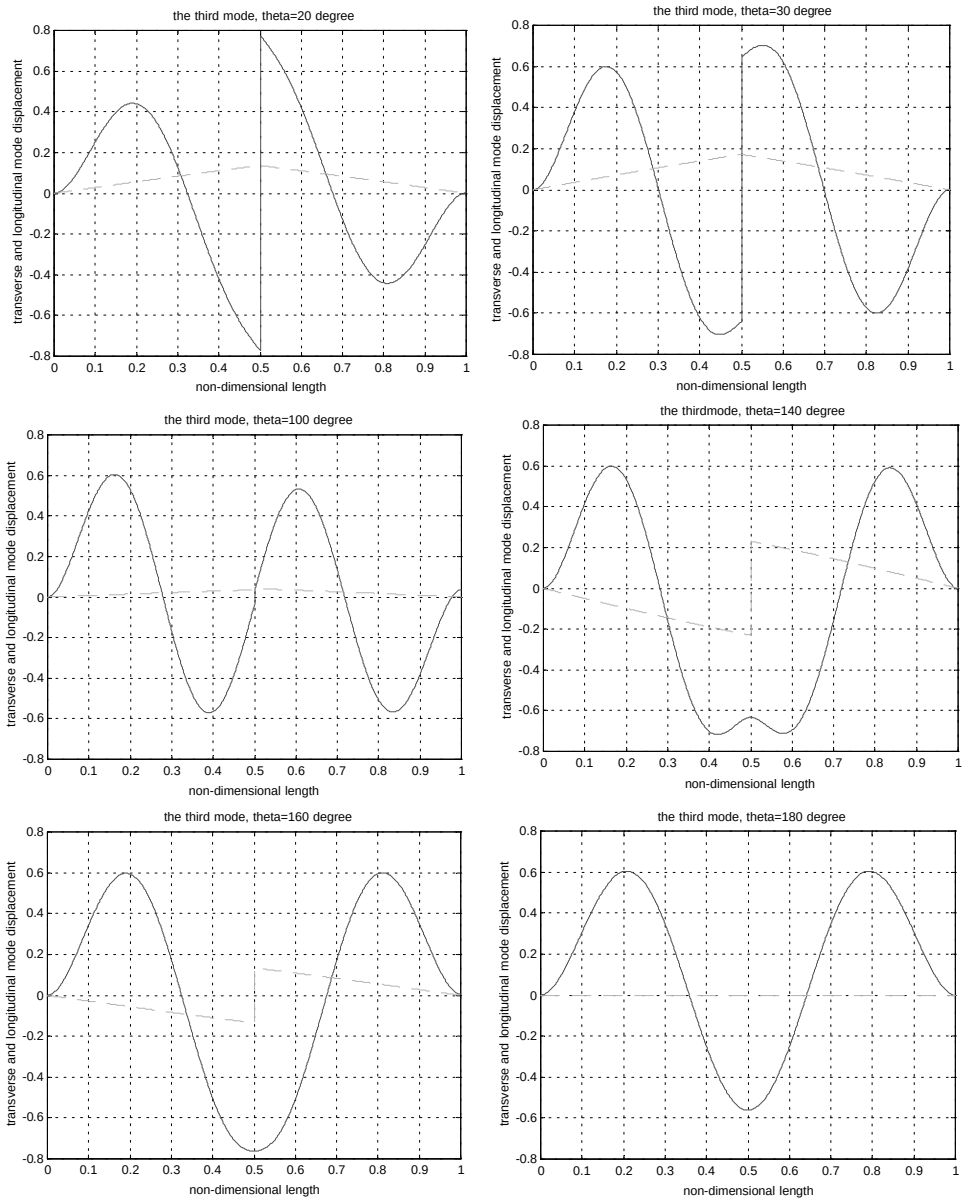

Fig. 11. Third mode shape for different θ_1 angles ($\theta_1 = 20^\circ, 30^\circ, 100^\circ, 140^\circ, 160^\circ$ and 180°): solid curve, transverse displacement; dashed curve, longitudinal displacement.

Unlike all the other methods, in which the dimensions of the matrix increase with the complexity of the structure, there are only six undetermined coefficients in the method proposed in this study. The main feature of this method is to decrease the dimension of the matrix involved in the finite element method and certain other analytical methods.

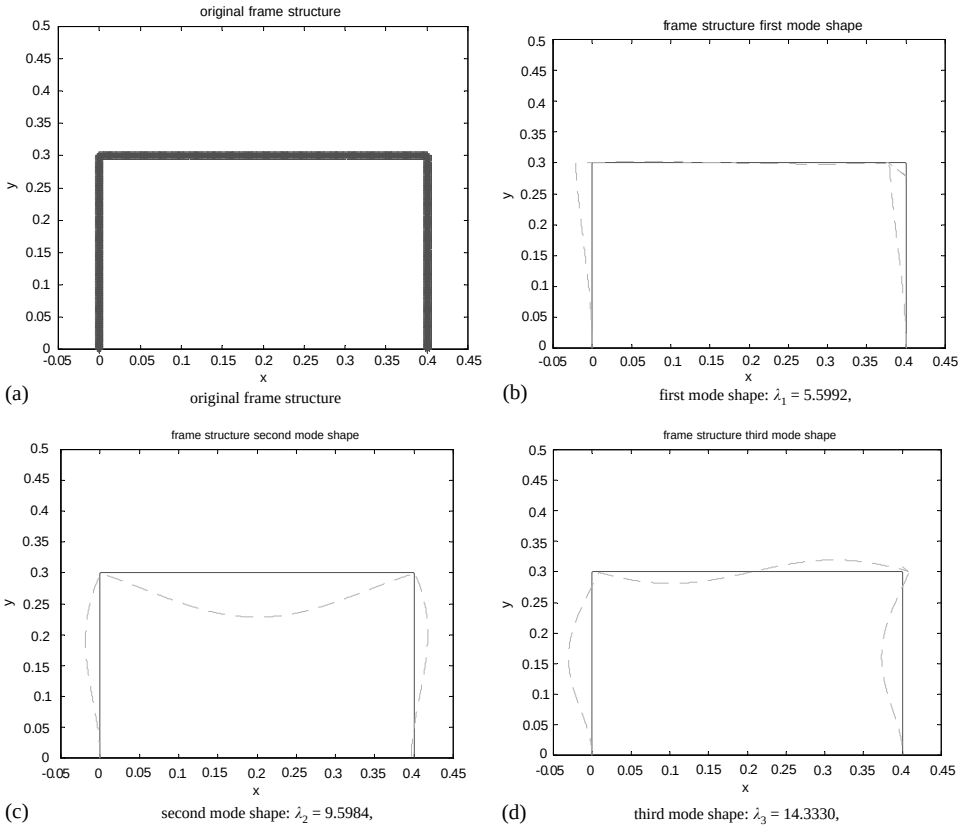

Fig. 12. Lowest three eigensolutions of a multi-angle frame structure.

Acknowledgements

The authors gratefully acknowledge the support of the National Science Council of Taiwan, R.O.C. under grant number NSC 90-2745-P-212-003. The authors also wish to express appreciation to Dr. Cheryl Rutledge for her editorial assistance.

Appendix A. Transfer matrix derivation

The compatibility conditions across the ith angle ($i = 1, 2, \ldots, K$) are represented in Eqs. (14a)–(14f).

From Eq. (14a),

$$w_{i+1}(x_i^+) = -w_i(x_i^-)\cos\theta_i + v_i(x_i^-)\sin\theta_i,$$
$$w_{i+1}(x_i^+) = B_{i+1} + D_{i+1},$$
$$w_i(x_i^-) = A_i \sin\lambda l_i + B\cos\lambda l_i + C_i \sinh\lambda l_i + D_i \cosh\lambda l_i,$$
$$v_i(x_i^-) = E_i \sin a\lambda^2 l_i + F_i \cos a\lambda^2 l_i,$$

$$B_{i+1} + D_{i+1} = -(A_i \sin \lambda l_i + B_i \cos\lambda l_i + C_i \sinh \lambda l_i + D_i \cosh \lambda l_i) \cos \theta_i + (E_i \sin a\lambda^2 l_i + F_i \cos a\lambda^2 l_i) \sin \theta_i, \quad i = 1, 2, \ldots, K. \tag{A.1}$$

From Eq. (14b),

$$v_{i+1}(x_i^+) = -w_i(x_i^-) \sin \theta_i - v_i(x_i^-) \cos \theta_i,$$
$$v_{i+1}(x_i^+) = F_{i+1},$$

$$F_{i+1} = -(A_i \sin \lambda l_i + B_i \cos \lambda l_i + C_i \sinh \lambda l_i + D_i \cosh \lambda l_i) \sin \theta_i - (E_i \sin a\lambda^2 l_i + F_i \cos a\lambda^2 l_i) \cos \theta_i, \quad i = 1, 2, \ldots, K. \tag{A.2}$$

From Eq. (14c),

$$w'_{i+1}(x_i^+) = w'_i(x_i^-),$$
$$w'_{i+1}(x_i^+) = A_{i+1}\lambda + C_{i+1}\lambda,$$
$$w'_i(x_i^-) = A_i\lambda \cos \lambda l_i - B_i\lambda \sin \lambda l_i + C_i\lambda \cosh \lambda l_i + D_i\lambda \sinh \lambda l_i,$$

$$A_{i+1} + C_{i+1} = A_i \cos \lambda l_i - B_i \sin \lambda l_i + C_i \cosh \lambda l_i + D_i \sinh \lambda l_i, \quad i = 1, 2, \ldots, K. \tag{A.3}$$

From Eq. (14d),

$$w''_{i+1}(x_i^+) = w''_i(x_i^-),$$
$$w''_{i+1}(x_i^+) = -B_{i+1}\lambda^2 + D_{i+1}\lambda^2,$$

$$w''_i(x_i^-) = -A_i\lambda^2 \sin \lambda l_i - B_i\lambda^2 \cos \lambda l_i + C_i\lambda^2 \sinh \lambda l_i + D_i\lambda^2 \cosh \lambda l_i - B_{i+1} + D_{i+1} = -A_i \sin \lambda l_i - B_i \cos \lambda l_i + C_i \sin \lambda l_i + D_i \cosh \lambda l_i, \quad i = 1, 2, \ldots, K. \tag{A.4}$$

From Eq. (14e),

$$w'''_{i+1}(x_i^+) = -w'''_i(x_i^-) \cos \theta_i - \frac{AL^2}{I} v'_i(x_i^-) \sin \theta_i,$$
$$w'''_{i+1}(x_i^+) = -A_{i+1}\lambda^3 + C_{i+1}\lambda^3,$$
$$w'''_i(x_i^-) = -A_i\lambda^3 \cos \lambda l_i + B_i\lambda^3 \sin \lambda l_i + C_i\lambda^3 \cosh \lambda l_i + D_i\lambda^3 \sinh \lambda l_i,$$

$$v'_i(x_i^-) = E_i a\lambda^2 \cos a\lambda^2 l_i - F_i a\lambda^2 \sin a\lambda^2 l_i,$$

$$-A_{i+1} + C_{i+1} = -(-A_i \cos \lambda l_i + B_i \sin \lambda l_i + C_i \cosh \lambda l_i + D_i \sinh \lambda l_i) \cos \theta_i - \frac{aAL^2}{I\lambda}(E_i \cos a\lambda^2 l_i - F_i \sin a\lambda^2 l_i) \sin \theta_i, \quad i = 1, 2, \ldots, K. \tag{A.5}$$

Here

$$a = \sqrt{\frac{I}{A}} \frac{1}{L}$$

so

$$\frac{aAL^2}{I\lambda} = \sqrt{\frac{AL^2}{I}}\frac{1}{\lambda} = \frac{\sqrt{12}}{(H/L)\lambda} \quad \text{(for square cross-section)}.$$

From Eq. (14f),

$$v'_{i+1}(x_i^+) = \frac{I}{AL^2} w'''_i(x_i^-)\sin\theta_i - v'_i(x_i^-)\cos\theta_i,$$

$$v'_{i+1}(x_i^+) = E_{i+1}a\lambda^2,$$

$$\begin{aligned} E_{i+1} &= \frac{I\lambda}{aAL^2}(-A_i\cos\lambda l_i + B_i\sin\lambda l_i + C_i\cosh\lambda l_i + D_i\sinh\lambda l_i)\sin\theta_i \\ &\quad - (E_i\cos a\lambda^2 l_i - F_i\sin a\lambda^2 l_i)\cos\theta_i \\ &= \frac{1}{\sqrt{12}}\left(\frac{H}{L}\right)\lambda(-A_i\cos\lambda l_i + B_i\sin\lambda l_i + C_i\cosh\lambda l_i + D_i\sinh\lambda l_i)\sin\theta_i \\ &\quad - (E_i\cos a\lambda^2 l_i - F_i\sin a\lambda^2 l_i)\cos\theta_i, \quad i = 1, 2, \ldots, K. \end{aligned} \tag{A.6}$$

Solving for Eqs. (A.1)–(A.6) leads to the following recursion formulae for the constants A_{i+1}, B_{i+1}, C_{i+1}, D_{i+1}, E_{i+1} and F_{i+1}:

$$\begin{Bmatrix} A_{i+1} \\ B_{i+1} \\ C_{i+1} \\ D_{i+1} \\ E_{i+1} \\ F_{i+1} \end{Bmatrix} = \begin{bmatrix} t_{11} & t_{12} & t_{13} & t_{14} & t_{15} & t_{16} \\ \vdots & & & & & \\ \vdots & & & & & \\ \ldots & & & & t_{65} & t_{66} \end{bmatrix}^{(i)} \begin{Bmatrix} A_i \\ B_i \\ C_i \\ D_i \\ E_i \\ F_i \end{Bmatrix} = \underline{T}^{(i)}_{6\times 6} \begin{Bmatrix} A_i \\ B_i \\ C_i \\ D_i \\ E_i \\ F_i \end{Bmatrix}, \quad i = 1, 2, \ldots, K.$$

Here, $\underline{T}^{(i)}_{6\times 6}$ is a transfer matrix composed of the elements:

$$t_{11} = \tfrac{1}{2}[\cos\lambda l_i(1-\cos\theta_i)], \qquad t_{12} = \tfrac{-1}{2}[\sin\lambda l_i(1-\cos\theta_i)],$$

$$t_{13} = \tfrac{1}{2}[\cosh\lambda l_i(1+\cos\theta_i)], \qquad t_{14} = \tfrac{1}{2}[\sinh\lambda l_i(1+\cos\theta_i)],$$

$$t_{15} = \frac{1}{2}\left[\frac{\sqrt{12}}{(H/L)\lambda}\cos a\lambda^2 l_i\sin\theta_i\right], \qquad t_{16} = \frac{-1}{2}\left[\frac{\sqrt{12}}{(H/L)\lambda}\sin a\lambda^2 l_i\sin\theta_i\right],$$

$$t_{21} = \tfrac{1}{2}[\sin\lambda l_i(1-\cos\theta_i)], \qquad t_{22} = \tfrac{1}{2}[\cos\lambda l_i(1-\cos\theta_i)],$$

$$t_{23} = \tfrac{-1}{2}[\sinh\lambda l_i(1+\cos\theta_i)], \qquad t_{24} = \tfrac{-1}{2}[\cosh\lambda l_i(1+\cos\theta_i)],$$

$$t_{25} = \tfrac{1}{2}[\sin a\lambda^2 l_i\sin\theta_i], \qquad t_{26} = \tfrac{1}{2}[\cos a\lambda^2 l_i\sin\theta_i],$$

$$t_{31} = \tfrac{1}{2}[\cos\lambda l_i(1+\cos\theta_i)], \qquad t_{32} = \tfrac{-1}{2}[\sin\lambda l_i(1+\cos\theta_i)],$$

$$t_{33} = \tfrac{1}{2}[\cosh\lambda l_i(1-\cos\theta_i)], \qquad t_{34} = \tfrac{1}{2}[\sinh\lambda l_i(1-\cos\theta_i)],$$

$$t_{35} = \frac{-1}{2}\left[\frac{\sqrt{12}}{(H/L)\lambda}\cos a\lambda^2 l_i \sin\theta_i\right], \qquad t_{36} = \frac{1}{2}\left[\frac{\sqrt{12}}{(H/L)\lambda}\sin a\lambda^2 l_i \sin\theta_i\right],$$

$$t_{41} = \tfrac{-1}{2}[\sin\lambda l_i(1+\cos\theta_i)], \qquad t_{42} = \tfrac{-1}{2}[\cos\lambda l_i(1+\cos\theta_i)],$$

$$t_{43} = \tfrac{1}{2}[\sinh\lambda l_i(1-\cos\theta_i)], \qquad t_{44} = \tfrac{1}{2}[\cosh\lambda l_i(1-\cos\theta_i)],$$

$$t_{45} = \tfrac{1}{2}[\sin a\lambda^2 l_i\sin\theta_i], \qquad t_{46} = \tfrac{1}{2}[\cos a\lambda^2 l_i\sin\theta_i],$$

$$t_{51} = \frac{-1}{\sqrt{12}}\left(\frac{H}{L}\right)\lambda\cos\lambda l_i\sin\theta_i, \qquad t_{52} = \frac{1}{\sqrt{12}}\left(\frac{H}{L}\right)\lambda\sin\lambda l_i\sin\theta_i,$$

$$t_{53} = \frac{1}{\sqrt{12}}\left(\frac{H}{L}\right)\lambda\cosh\lambda l_i\sin\theta_i, \qquad t_{54} = \frac{1}{\sqrt{12}}\left(\frac{H}{L}\right)\lambda\sinh\lambda l_i\sin\theta_i,$$

$$t_{55} = -\cos a\lambda^2 l_i\cos\theta_i, \qquad t_{56} = \sin a\lambda^2 l_i\cos\theta_i,$$

$$t_{61} = -\sin\lambda l_i\sin\theta_i, \qquad t_{62} = -\cos\lambda l_i\sin\theta_i,$$

$$t_{63} = -\sinh\lambda l_i\sin\theta_i, \qquad t_{64} = -\cosh\lambda l_i\sin\theta_i,$$

$$t_{65} = -\sin a\lambda^2 l_i\cos\theta_i, \qquad t_{66} = -\cos a\lambda^2 l_i\cos\theta_i.$$

References

[1] A.Y.T. Leung, Dynamic stiffness for structures with distributed deterministic or random loads, Journal of Sound and Vibration 242 (3) (2001) 377–395.

[2] D.H. Moon, M.S. Choi, Vibration analysis for frame structures using transfer of dynamic stiffness coefficient, Journal of Sound and Vibration 234 (5) (2000) 725–736.

[3] N.S. Sehmi, Large Order Structural Eigenanalysis Techniques Algorithm for Finite Element Systems, Ellis Horwood, New York, 1989.

[4] M. Geradin, S.L. Chen, An exact model reduction technique for beam structures: combination of transfer and dynamic stiffness matrices, Journal of Sound and Vibration 185 (3) (1995) 431–440.

[5] M. Ohga, T. Shigematsu, T. Hara, Structural analysis by a combined finite element transfer matrix method, Computers and Structures 17 (1983) 321–326.

[6] L. Meirovitch, Fundamentals of Vibrations, International Edition, McGraw-Hill Higher Education, Singapore, 2001.

[7] W.C. Hurty, M.F. Rubinstein, Dynamics of Structures, Prentice-Hall, Englewood Cliffs, NJ, 1964.

[8] L. Meirovitch, Elements of Vibration Analysis International Edition, McGraw-Hill, Singapore, 1986.

[9] H.P. Lin, N.C. Perkins, Free vibration of complex cable/mass system: theory and experiment, Journal of Sound and Vibration 179 (1) (1995) 131–149.

[10] H.P. Lin, C.K. Chen, Analysis of cracked beams by transfer matrix method, The 25th National Conference on Theoretical and Applied Mechanics, Taichung, Taiwan, ROC, 2001, pp. 3123–3132.